



HAL
open science

Quinolinophenothiazine as electron rich fragment for RGB single-layer phosphorescent organic light-emitting diodes

Fabien Lucas, Denis Tondelier, Bernard Geffroy, Thomas Heiser, Olzhas Ibraikulov, Cassandre Quinton, Clement Brouillac, Nicolas Leclerc, Joëlle Rault-Berthelot, Cyril Poriel

► To cite this version:

Fabien Lucas, Denis Tondelier, Bernard Geffroy, Thomas Heiser, Olzhas Ibraikulov, et al.. Quinolinophenothiazine as electron rich fragment for RGB single-layer phosphorescent organic light-emitting diodes. *Materials Chemistry Frontiers*, In press, 5 (22), pp.8066-8077. 10.1039/D1QM01138C . cea-03355001

HAL Id: cea-03355001

<https://cea.hal.science/cea-03355001>

Submitted on 25 Oct 2021

HAL is a multi-disciplinary open access archive for the deposit and dissemination of scientific research documents, whether they are published or not. The documents may come from teaching and research institutions in France or abroad, or from public or private research centers.

L'archive ouverte pluridisciplinaire **HAL**, est destinée au dépôt et à la diffusion de documents scientifiques de niveau recherche, publiés ou non, émanant des établissements d'enseignement et de recherche français ou étrangers, des laboratoires publics ou privés.

Quinolinophenothiazine as Electron Rich Fragment for RGB Single-Layer Phosphorescent Organic Light-Emitting Diodes*

Fabien Lucas,^a Denis Tondelier,^b Bernard Geffroy,^{b,c} Thomas Heiser,^d Olzhas A. Ibraikulov,^d Cassandre Quinton,^a Clément Brouillac,^a Nicolas Leclerc,^c Joëlle Rault-Berthelot,^a and Cyril Poriel^{a*}

^a Univ Rennes, CNRS, ISCR-UMR CNRS 6226, F-35000 Rennes, France-
email: cyril.poriel@univ-rennes1.fr

^b LPICM, CNRS, Ecole Polytechnique, IPParis, 91128 Palaiseau, France

^c LICSEN, NIMBE, CEA, CNRS, Université Paris-Saclay, CEA Saclay, 91191 Gif-sur-Yvette Cedex, France

^d Laboratoire ICube, Université de Strasbourg, UMR CNRS 7357, 67087 Strasbourg, France

^e Institut de Chimie et Procédés pour l'Énergie, l'Environnement et la Santé (ICPEES), UMR CNRS 7515, 67087 Strasbourg, France

Keywords: high E_T host materials, single-layer phosphorescent organic light-emitting diode, *spiro* compounds, quinolinophenothiazine

Abstract

The quinolinophenothiazine (QPTZ) fragment is a phenylacridine bridged by a sulphur atom. Despite appealing properties induced by this bridging (*e.g.* strong electron rich character), this fragment remains almost unexplored to date in organic electronics. Based on this QPTZ fragment, we report herein a high efficiency host for the new generation of simplified Phosphorescent Organic Light-Emitting Diodes so called Single-Layer (SL-PhOLEDs). This host material is constructed on the association of an electron rich fragment (QPTZ), and an electron-deficient fragment (2,7-bis(diphenylphosphineoxide)-fluorene). This molecule displays all the necessary properties to be used in universal SL-PhOLEDs.

Red, green and blue SL-PhOLEDs were successfully fabricated and yielded an average external quantum efficiency of ca 10%. High luminances of ca 10000 cd/m² for red and blue devices and 40000 cd/m² for green devices were obtained. These luminances are higher than the best reported to date with structurally related analogues and highlight the strong interest of the QPTZ fragment in such devices. Thanks to its high HOMO level, the QPTZ unit also allows to decrease the threshold voltage, which is a key characteristic in the OLED technology.

This work shows the potential of the QPTZ fragment in the design of host materials for high performance single-layer PhOLEDs.

* *Dedicated to Bernard Geffroy on the occasion of his retirement*

Introduction

Since the last 30 years, the fantastic emergence of organic electronics is, in part, assignable to the design, the synthesis and the study of thousands of organic semi-conductors (OSCs) with properties fitting with the different electronic devices.¹⁻⁴ These OSCs are constructed thanks to the availability of many highly efficient molecular building blocks with specific properties (high electron and/or hole mobilities, large HOMO/LUMO gap, high quantum yield, high triplet state energy values....). In the field of Organic Light Emitting Diodes (OLEDs), the widely known electron rich PhenylAcridine (PA)⁵⁻⁶ (Chart 1) holds a special place as it is one of the most efficient building block reported to date due to its excellent properties in term of charge injection and transport.^{5, 7-11} Around this fragment, researchers have designed, in the last ten years, four other structurally related building units which are IndoloAcridine (IA),¹²⁻¹⁵ QuinolinoPhenoThiaZine (QPTZ),¹⁶⁻¹⁷ QuinolinoOxazine (QO)¹⁸⁻¹⁹ and QuinolinoAcridine (QA)^{10, 20} (Chart 1), which all display very different electronic properties. In these fragments, two phenyl units of the PA core are either linked by a carbon-carbon bond (IA) or bridged either by an oxygen (QO), a sulphur (QPTZ) or a carbon (QA) atom. These building blocks have successfully been incorporated in OSCs with improved device performances compared to the PA unit. For example, in the field of phosphorescent OLEDs (PhOLEDs), the potential of the QPTZ fragment to construct high efficiency host materials used in multi-layer PhOLEDs has been highlighted.¹⁶ Similarly, in 2019, Jiang, Liao and their coworkers have reported the great potential of the QO¹⁸⁻¹⁹ and QA^{10, 20} units in very high performance phosphorescent and TADF OLEDs. In the case of the QPTZ fragment, the key role played by the sulphur atom has been particularly highlighted over the years. Thus, compare to its PA counterpart, the QPTZ fragment displays a significant increase of the HOMO energy level and remarkably stable radical cations.¹⁶ This strong electron rich character finds its origin in the electron donating behaviour of the intracyclic sulphur atom, which fully drives the HOMO energy level.¹⁶ In 2018, the singular chiral properties of the QPTZ fragment have also been reported as a unique molecular tool to reach chiral OSCs.¹⁷ However, this molecular fragment, described more than 40 years ago,²¹ has never been used in the new generation of simplified PhOLEDs so-called *single-layer*. For the last twenty years, simplifying fluorescent²² and phosphorescent OLEDs²³ has indeed attracted the attention of many research groups worldwide. The goal is to bridge the gap between multi-layer PhOLEDs, which are highly efficient and widely described nowadays in literature^{11, 24-40} and the new generation of single-layer PhOLEDs (SL-PhOLEDs), which still presents low performance except for a few examples.^{7, 23, 41-43} Simplifying PhOLEDs will notably reduce the inherent complexity of the stack and its cost. More importantly, for the future ecological transition, simplifying electronic devices will help to reduce its environmental footprint. This is a central notion nowadays.

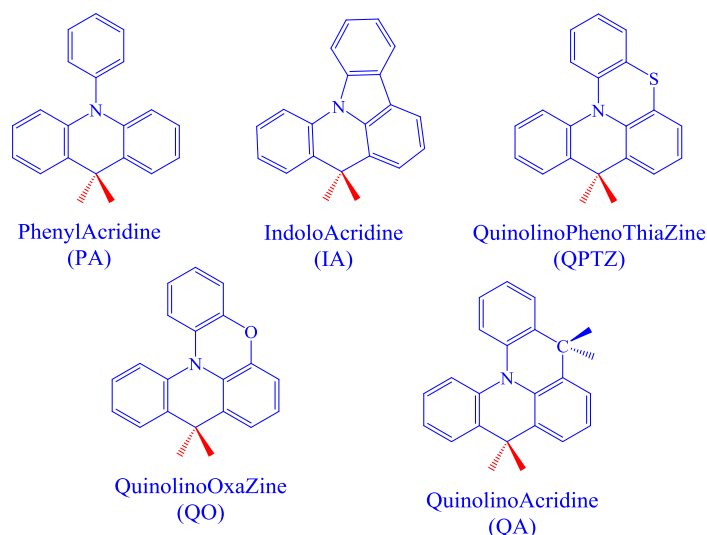


Chart 1: Phenylacridine (PA), indoloacridine (IA) quinolinophenothiazine (QPTZ), quinolinooxazine (QO), quinolinoacridine (QA)

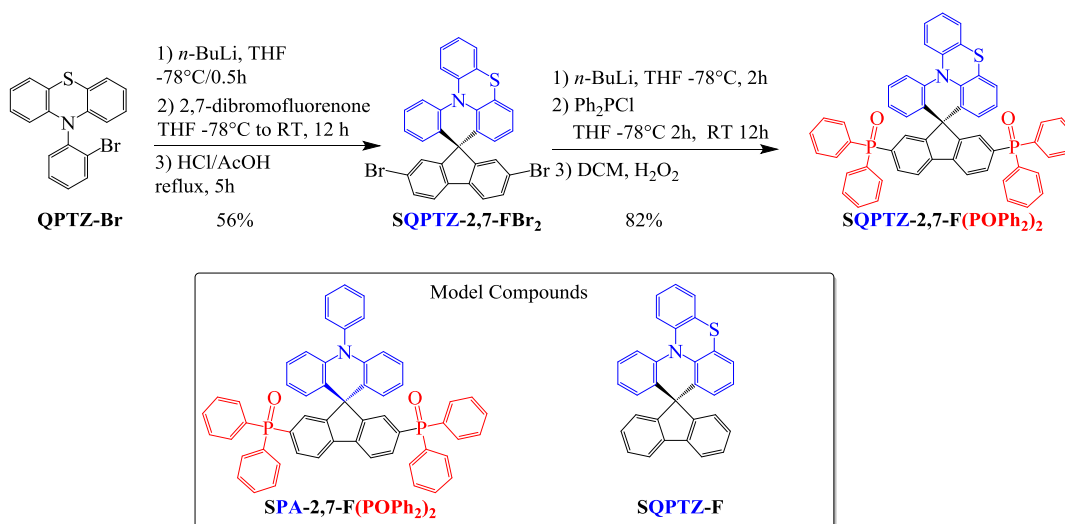
In this *single-layer* technology, the molecular design of the emissive layer undoubtedly drives the field. Recently, great advances have been reached with very high performance host materials reported in red, green and blue SL-PhOLEDs.^{7, 41-42} However, to date, there is only a very small number of high-efficiency host materials, which are compatible with red (R), green (G) and blue (B) SL-PhOLEDs.⁴¹ As the future of SL-PhOLEDs (and more generally organic electronics) strongly relies on the use of elementary molecular fragments, we wish to report herein the use of the QPTZ building block integrated in a universal host for RGB SL-PhOLEDs. The potential of the QPTZ fragment has been evaluated through the synthesis of a bipolar *spiro*-configured host, spiroquinolinophenothiazine-2,7-bis(diphenylphosphine oxide)-fluorene (**SQPTZ-2,7-F(POPh₂)₂**) constructed on the association of the QPTZ electron-rich fragment and the 2,7-(diphenylphosphine oxide)-fluorene electron-poor fragment.⁴⁴ This combination provides suitable mobilities, a high triplet energy (E_T) of 2.76 eV and high decomposition (T_d) and glass transition (T_g) temperatures. The HOMO energy level appears to be higher than structurally related PA compounds. RGB SL-PhOLEDs have finally been fabricated and display an average EQE of ca 10% and high luminances of ca 10000 cd/m² for red and blue devices and 40000 cd/m² for green devices. These luminances are higher than those reported for the structurally related PA host (named **SPA-2,7-F(POPh₂)₂**), which is the most efficient host material for SL-PhOLEDs reported to date.⁴¹ This highlights the strong interest of the QPTZ fragment in such devices. Thanks to its high HOMO level, the QPTZ unit also allows to decrease the threshold voltage of the devices compared to the structurally related PA host **SPA-2,7-F(POPh₂)₂**). All these characteristics open the way to the use of QPTZ fragment in the design of OSC for SL-PhOLEDs.

Results and discussion

Synthesis

SQPTZ-2,7-F(POPh₂)₂ has been synthesized through an efficient, short and high yielded two-step approach (Scheme 1). Reducing the synthetic chemistry steps is highly required to decrease the environmental footprint of electronic devices. The first step is a

classical lithium-bromine exchange on 10-(2-bromophenyl)-10H-phenothiazine (**QPTZ-Br**) (obtained from the copper catalysed Ullmann-Goldberg coupling of phenothiazine and 2-bromoiodobenzene), followed by a nucleophilic addition reaction in the presence of 2,7-dibromofluorenone. The fluorenone obtained (not isolated) is then involved in an intramolecular electrophilic substitution to give the spiroquinolinophenothiazine-2,7-dibromofluorene (**SQPTZ-2,7-FBr₂**) in a yield of 56%. Incorporation of the diphenylphosphine oxide fragments is finally performed through a double lithium-bromine exchange on **SQPTZ-2,7-FBr₂**, followed by a nucleophilic addition with chlorodiphenylphosphine. The resulting diphenylphosphine compound (not isolated) is further oxidized by H₂O₂ to give **SQPTZ-2,7-F(POPh₂)₂** with a yield of 82%.



Scheme 1. Synthesis of **SQPTZ-2,7-F(POPh₂)₂** and molecular structure of model compounds **SPA-2,7-F(POPh₂)₂** and **SQPTZ-F**

In order to precisely study the impact of the incorporation of the QPTZ electron-rich fragment within **SQPTZ-2,7-F(POPh₂)₂**, two model compounds will also be studied, spiroquinolinophenothiazine-fluorene **SQPTZ-F**, which corresponds to **SQPTZ-2,7-F(POPh₂)₂** without the diphenylphosphine oxide moieties, and spirophenylacridine-2,7-bis(diphenylphosphine oxide)-fluorene (**SPA-2,7-F(POPh₂)₂**),⁴¹ which is the analogue of **SQPTZ-2,7-F(POPh₂)₂** but possessing a PA fragment instead of a QPTZ fragment. Note that **SPA-2,7-F(POPh₂)₂** is, in 2021, the host material displaying the highest performance in RGB SL-PhOLEDs (average EQE above 14% for the three colours).⁴¹

Electrochemical properties

The electrochemical properties of **SQPTZ-2,7-F(POPh₂)₂**, **SQPTZ-F** and **SPA-2,7-F(POPh₂)₂** have been first investigated by cyclic voltammetry (CV) in CH₂Cl₂ for oxidation (Figure 1, right) and in DMF for reduction (Figure 1, left); potentials are given versus a saturated calomel electrode (SCE).

The electron rich character of the QPTZ fragment is the most important feature to unravel herein. In oxidation (Figure 1, right), **SQPTZ-2,7-F(POPh₂)₂** presents three oxidation waves with peak potentials $E^1/E^2/E^3$ recorded at 0.96/1.54/1.69 V (Figure 1, black line). Only the first oxidation process is reversible and assigned to an electron transfer centred on the QPTZ unit (See HOMO density in Figure 2). The model compound **SQPTZ-F** presents two reversible waves at 0.89 and 1.61 V (Figure 1, red line). As a fluorene moiety is oxidised at potential more anodic than 1.7 V and through an irreversible electron transfer, typically leading to electrodeposition processes,⁴⁵⁻⁴⁸ the two first oxidation waves of **SQPTZ-F** have

been assigned to two single-electron transfers involving the QPTZ core. As observed for **SQPTZ-2,7-F(POPh₂)₂**, the HOMO of **SQPTZ-F** is exclusively centred on the QPTZ fragment (Figure 2). Figure 1 also presents the oxidation of **SPA-2,7-F(POPh₂)₂**, displaying a first wave at $E^1 = 1.06$ V (Figure 1, blue line).¹²

Several conclusions can be drawn. First, we note that the phosphine oxides attached to the fluorene in **SQPTZ-2,7-F(POPh₂)₂** lead to a 70 mV positive shift compared to that of QPTZ core in **SQPTZ-F**. Thus, despite a *spiro* carbon connection, the QPTZ and fluorene moieties are not fully electronically separated. Second, the first oxidation of the QPTZ fragment remarkably occurs at a less anodic potential than that of PA core (shift of 100 mV). This strong electron rich character finds its origin in the electron donating behaviour of the intracyclic sulphur atom, which fully drives the HOMO energy level of these OSCs (Figure 2). The third important feature in the electrochemistry of QPTZ-based compounds is linked to the reversibility of the waves. Indeed, in both **SQPTZ-2,7-F(POPh₂)₂** and **SQPTZ-F**, the reversibility of the first oxidation wave indicates an efficient delocalization of the charges within the QPTZ core. This behaviour is not found for the structurally analogues based on the PA core, showing the great influence of the intracyclic sulphur atom on the electrochemical properties not only in terms of potential but also of stability of the cationic species.

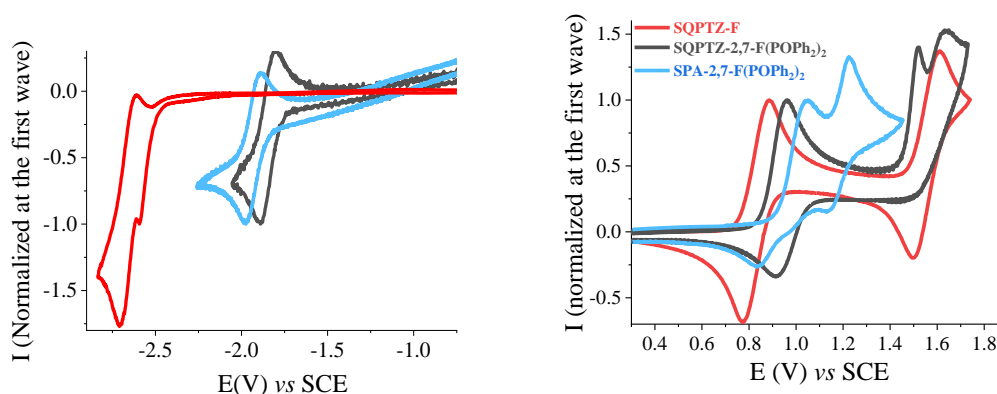


Figure 1. Cyclic voltammetry in reduction (Left, DMF + Bu₄NPF₆ 0.1 M, sweep-rate 100 mV.s⁻¹) and in oxidation (Right, CH₂Cl₂ + Bu₄NPF₆ 0.2 M, sweep-rate 100 mV.s⁻¹) of **SQPTZ-2,7-F(POPh₂)₂**, **SQPTZ-F** and **SPA-2,7-F(POPh₂)₂**.

We determined the HOMO energy level of **SQPTZ-2,7-F(POPh₂)₂** at -5.25 eV, higher than that of **SPA-2,7-F(POPh₂)₂** (-5.33 eV),¹² confirming the strong electron-rich nature of the QPTZ fragment. It should also be noted that the HOMO energy level of **SQPTZ-F** (-5.16 eV) is higher than that of **SQPTZ-2,7-F(POPh₂)₂**, translating the non-negligible influence of the acceptor unit on the HOMO level *via* the *spiro* bridge. The higher HOMO energy level of **SQPTZ-2,7-F(POPh₂)₂** vs **SPA-2,7-F(POPh₂)₂** should favour the hole injection, which is beneficial for OLED applications (see below).

In reduction (Figure 1, left), **SQPTZ-F** displays an irreversible wave at very negative potential, -2.52 V. In **SQPTZ-2,7-F(POPh₂)₂**, the electron accepting capability of the two phosphine oxides significantly increases the reduction potential recorded at less negative value, -1.94 V. It is important to note that the incorporation of phosphine oxide units on the fluorene core allows obtaining a reversible wave. The PA analogue **SPA-2,7-F(POPh₂)₂** displays a similar behaviour with a first reversible wave at -1.98 V, confirming that the reversibility is induced by the phosphine oxide units. Thus, the cathodic exploration indicates that the reduction of the three molecules is fully governed by the acceptor part (diphenylphosphine oxide-fluorene) with nevertheless an influence of the donor part. To sum

up, among the three molecules, only **SQPTZ-2,7-F(POPh₂)₂** displays both a reversible oxidation and a reversible reduction wave. The LUMO levels obtained from the onset reduction potential are respectively evaluated at -2.60, -1.89 and -2.55 eV for **SQPTZ-2,7-F(POPh₂)₂**, **SQPTZ-F** and **SPA-2,7-F(POPh₂)₂**. Thus, for the two phosphine oxides-based compounds, one can note that the lowest LUMO and the highest HOMO are obtained with **SQPTZ-2,7-F(POPh₂)₂**, which therefore presents a more contracted electrochemical gap (ΔE_{el}) than **SPA-2,7-F(POPh₂)₂** counterpart (2.65 vs 2.78 eV). This is one of the advantages of the QPTZ fragment and a key point for the application targeted herein. This gap contraction will contribute to decrease the threshold voltage of the SL-PhOLEDs as detailed below.

Note that, in these materials, the HOMO is driven by the donor part (QPTZ or PA) and the LUMO by the acceptor part (diphenylphosphine oxide-fluorene). This is in agreement with molecular modelling (b3lyp 6-311+G(d, p)), which shows that electronic delocalization of the HOMO and LUMO are spread out on the corresponding fragments (Figure 2). There is hence a spatial separation between the HOMO and the LUMO levels, which allows to control the electronic properties and to gather within a single material the HOMO/LUMO energy levels of the constituting building blocks, a short π -conjugation pathway and a high E_T .

Photophysical properties

The strong structural similitude between **SQPTZ-2,7-F(POPh₂)₂** and **SPA-2,7-F(POPh₂)₂** is reflected by their very similar absorption spectrum (Figure 3, top-left). The absorption is located in the near UV and constituted of four main bands (ca 321/323, 309/310, 294/295 and 282/283 nm). Both compounds present a broad band at ca 321/323 nm assigned in the light of Time-Dependent DFT to a transition with both orbitals centred on the fluorene (HOMO-1 \rightarrow LUMO for **SPA-2,7-F(POPh₂)₂** and HOMO-2 \rightarrow LUMO for **SQPTZ-2,7-F(POPh₂)₂**), Figure 2. This transition drives the optical gap of these two materials (ΔE^{opt} of ca 3.75 eV). Oppositely, the band at 309/310 nm corresponds to a transition with both orbitals mainly centred on the donor unit (QPTZ or PA). Thus, TD-DFT indicates that the main transitions in these compounds are centred on the same fragment, either the donor or the acceptor (Figure 2). However, the first excited state corresponds to a forbidden HOMO-LUMO transition ($f=0$), not observed experimentally. This originates from the spatial separation of HOMO and LUMO levels with HOMO localized on the donor fragment and LUMO on the acceptor core, Figure 2, leading to a through-space forbidden transition.⁵ This characteristic allows to keep a short π -conjugated pathway, essential in the design of host materials.⁵

Note that the spectrum of **SQPTZ-F** is not significantly different with a main band at 308 nm, shifted by 13/15 nm compared to the above discussed compounds. This transition is due to a HOMO \rightarrow LUMO+4 transition, with both orbitals mainly centred on the QPTZ core. As detailed above, in the case of **SQPTZ-2,7-F(POPh₂)₂** and **SPA-2,7-F(POPh₂)₂**, the highest transition was induced by the fluorene/diphenylphosphine oxide fragment. Thus, removing the phosphine oxide fragments leads to a hypsochromic shift of the main band and in turn modifies the molecular orbitals involved in the main transition. This is due to their conjugation with the fluorene core. However, the main characteristic is kept identical, namely a forbidden HOMO-LUMO transition due to the spatial separation of these orbitals.

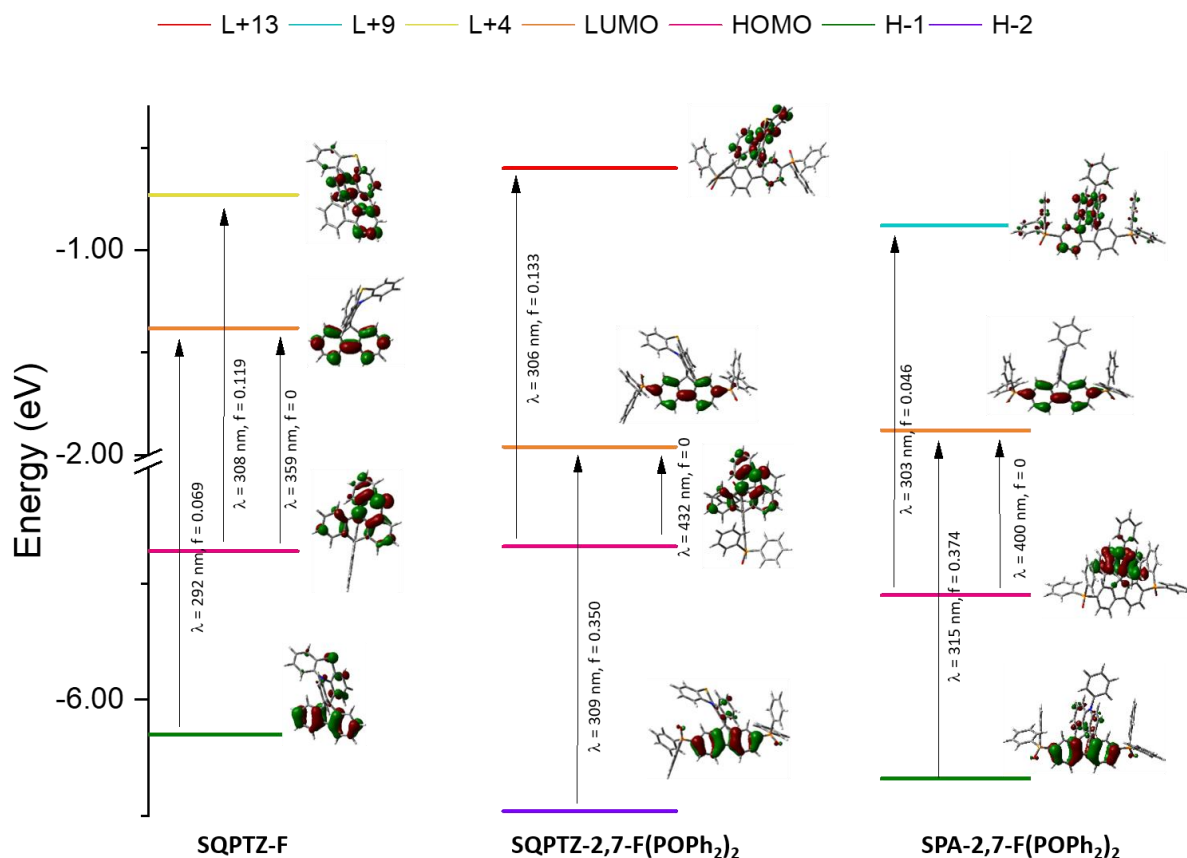


Figure 2. Representation of the energy levels and the main molecular orbitals involved in the electronic transitions of **SQPTZ-F**, **SQPTZ-2,7-F(POPh₂)₂** and **SPA-2,7-F(POPh₂)₂** obtained by TD-DFT b3lyp and the 6-311+G(d, p) basis set on the geometry of S₀, shown with an isovalues of 0.04 [e bohr⁻³]^{1/2} (for clarity purpose, only the main contribution for each transition is shown, details provided in SI).

In fluorescence spectroscopy (cyclohexane, Figure 3-Top right), the three compounds are very weak emitters with quantum yields below 0.01 (Table 1), in accordance with the spatial separation of HOMO and LUMO and a forbidden S₀→S₁ transition. This characteristic is usually found in the most efficient bipolar host materials reported to date.⁴¹

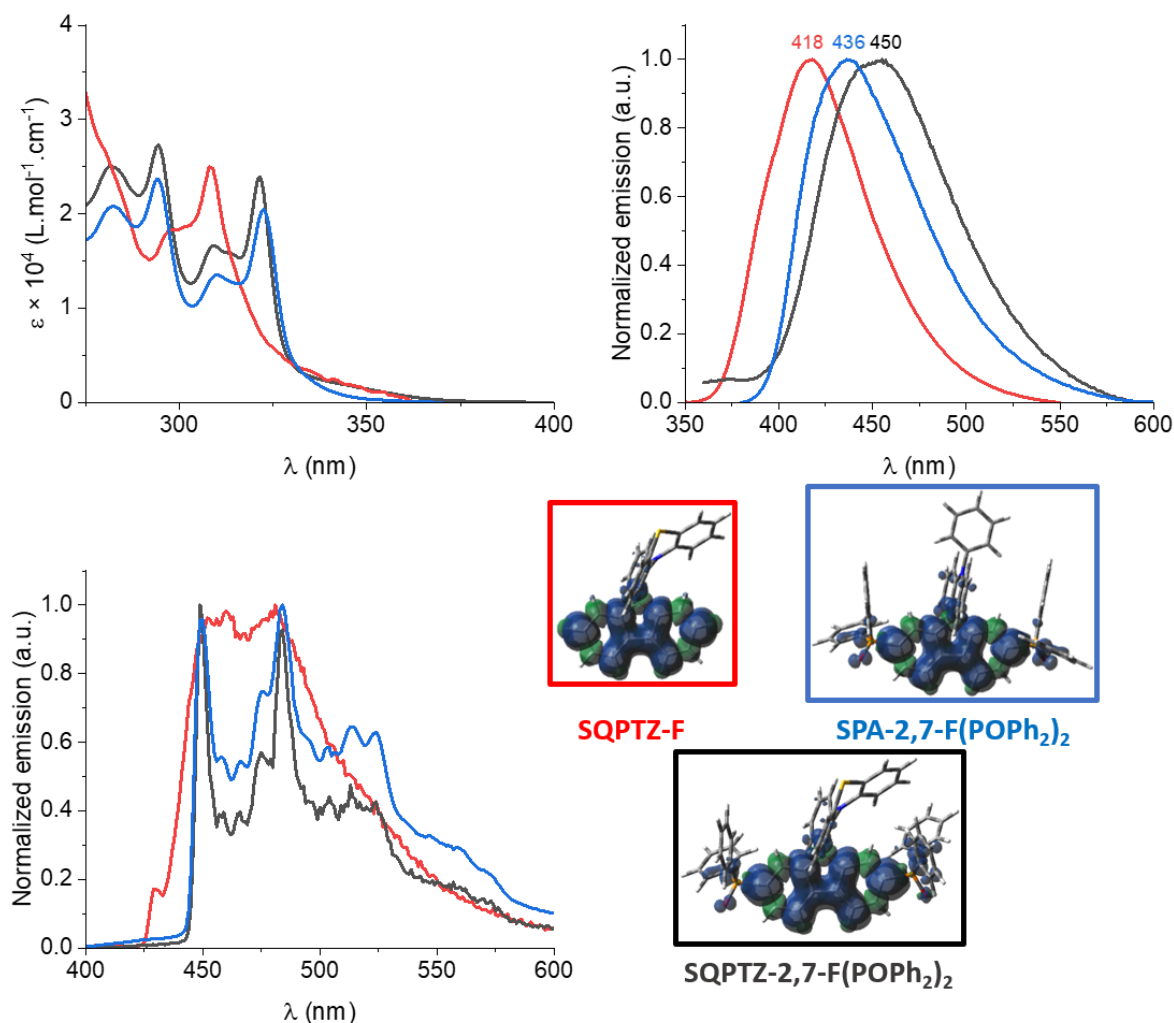


Figure 3. **SQPTZ-2,7-F(POPh₂)₂**, (black lines) **SQPTZ-F** (red lines) and **SPA-2,7-F(POPh₂)₂** (blue lines). UV-Vis absorption spectra in cyclohexane (Top-left). Normalized emission spectra at room temperature in cyclohexane, $\lambda_{\text{exc}} = 310$ nm (Top-right). Emission spectra at 77 K in 2-MeTHF ($\lambda_{\text{exc}} = 310$ nm) normalized at the phosphorescence maxima (Bottom-left). Triplet spin density distribution (TD-DFT, b3lyp/6-311+g(d, p), isovalue 0.0005, Bottom-right).

The emission spectra are unresolved and we note a gradual red shift of their maxima from **SQPTZ-F** (418 nm) to **SPA-2,7-F(POPh₂)₂** (436 nm), and to **SQPTZ-2,7-F(POPh₂)₂** (450 nm). Thus, oppositely to their absorption spectra, **SPA-2,7-F(POPh₂)₂** and **SQPTZ-2,7-F(POPh₂)₂** display different emission spectra. This can be assigned to the more electron rich nature of the QPTZ fragment, which induces a stronger photoinduced intramolecular charge transfer (ICT). Solvatochromic experiments allow a deeper understanding of the photophysical properties through the determination of the polarity of the excited states (Figure 4). Indeed, the emission maximum of **SQPTZ-F** in polar (MeCN or MeOH) or apolar solvent (cyclohexane) is only very weakly shifted. This is in accordance with a very weak ICT (and a transition occurring in only one fragment involved, namely QPTZ, Figure 4, left). **SQPTZ-2,7-F(POPh₂)₂** displays a very different behaviour with an impressive red shift of 139 nm between cyclohexane (452 nm) and MeOH (591 nm) highlighting a strong photoinduced ICT, Figure 4, middle. One can note, in the case of **SQPTZ-2,7-F(POPh₂)₂**, the presence of a shoulder at low wavelength (MeOH), which can sign the existence of a locally excited state in addition to the ICT state. The PA analogue **SPA-2,7-F(POPh₂)₂** displays a weaker

solvatochromic effect, with a shift of 99 nm between cyclohexane (439 nm) and MeOH (538 nm), translating the different electron rich characters between PA and QPTZ (Figure 4-right).

The difference ($\Delta\mu$) between the dipole moment at the ground state (μ) and at the first excited state (μ^*) have been evaluated using the Lippert-Mataga formalism. $\Delta\mu$ of 3.5, 34.2 and 31.2 D have been measured (the dipole moments at the ground state have been obtained by DFT calculations, 1.5, 5.9 and 9.3 D) for **SQPTZ-F**, **SQPTZ-2,7-F(POPh₂)₂** and **SPA-2,7-F(POPh₂)₂**, respectively, see SI). These $\Delta\mu$ data translate the different polarity of the three fluorophores at the excited state ($\mu^* = 5.0, 40.1$ and 40.5 D resp.). The strong solvatochromic effect (Figure 4) and the corresponding high $\Delta\mu$ observed for **SQPTZ-2,7-F(POPh₂)₂** and **SPA-2,7-F(POPh₂)₂** are indicative of a significant photoinduced ICT whereas the negligible solvatochromic effect and the corresponding low $\Delta\mu$ observed for **SQPTZ-F** are indicative of a very weak photoinduced ICT. Thus, one can note that (i) the QPTZ fragment provides the highest $\Delta\mu$ due to its electron-rich behaviour higher than that of the PA analogue **SPA-2,7-F(POPh₂)₂** and (ii) the acceptor unit can drastically change the electronic properties of QPTZ based compounds.

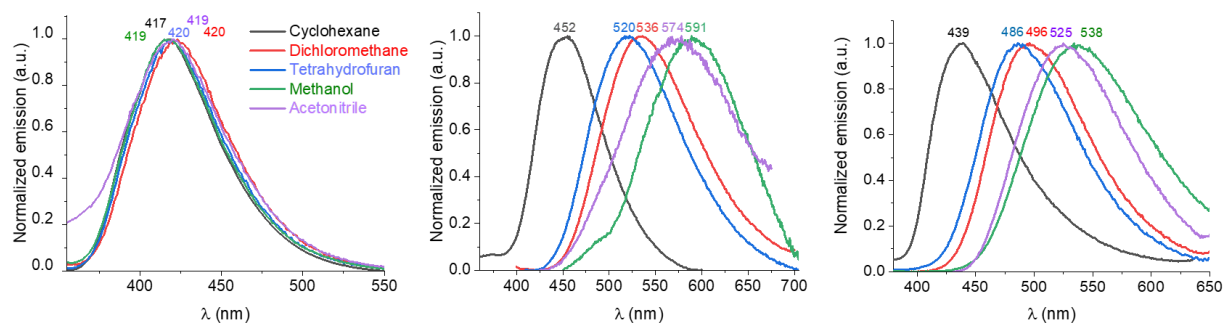


Figure 4. Emission spectra in different solvents of **SQPTZ-F** (Left), **SQPTZ-2,7-F(POPh₂)₂** (middle) and **SPA-2,7-F(POPh₂)₂** (Right).

At 77 K, the emission spectra of both **SQPTZ-2,7-F(POPh₂)₂** and **SPA-2,7-F(POPh₂)₂** show a phosphorescence contribution, with a first band centred at around 450 nm leading to a high triplet state energy level E_T of 2.76 eV (Figure 3, Bottom-left). A very long lifetime, $\tau = 3.4$ and 3.1 s for **SQPTZ-2,7-F(POPh₂)₂** and **SPA-2,7-F(POPh₂)₂** respectively (Table 1), is measured confirming an emission from the T1 state. These phosphorescence contributions are very similar, in accordance with an E_T value fully governed by the bis(diphenylphosphineoxide)-fluorene fragment. This is confirmed by the triplet spin density distribution (SDD) obtained by TD-DFT (b3lyp/6-311+g(d, p), Figure 3, Bottom-right), which shows for both a triplet state located on this fragment with no contribution of the QPTZ or PA unit. The spin density is mainly located on the fluorene core with nevertheless a non-negligible contribution of the phosphine oxide fragments. Thus, in this type of *D-Spiro-A* design,^{5, 12, 49} the donor unit can be easily modified (to adjust for example the HOMO energy level), without decreasing the E_T . This is an interesting feature for further molecular design of host materials.

Model compound **SQPTZ-F** displays a less resolved phosphorescence contribution with a SDD exclusively distributed on the fluorene. Thus, in the three compounds, the E_T is mainly imposed by the fluorene core. The E_T of **SQPTZ-F** is measured at 2.88 eV, 0.12 eV higher than those of both **SQPTZ-2,7-F(POPh₂)₂** and **SPA-2,7-F(POPh₂)₂**. This shows that the incorporation of the two phosphine oxide units significantly decreases the E_T due to their

conjugations with the fluorene backbone. It should finally be noted that the E_T of **SQPTZ-F** is very similar to the value reported for the fluorene unit itself, 2.93 eV.⁵⁰ The decrease of 0.05 eV is due to the interaction with the QPTZ fragment by *spiro*-conjugation as previously observed with other *spiro* compounds.⁵¹

Table 1 Selected electronic data of **SQPTZ-2,7-F(POPh₂)₂**, **SQPTZ-F** and **SPA-2,7-F(POPh₂)₂**

	SQPTZ-2,7-F(POPh₂)₂	SQPTZ-F	SPA-2,7-F(POPh₂)₂
$\lambda_{\text{abs max}} [\text{nm}]^a$	321 (2.4); 309 (1.7); 294 (2.7); 282 (2.5)	308 (2.5); 298 (1.8)	323 (2.5); 310 (1.3); 295 (2.4); 283 (2.1)
$(\epsilon \times 10^4 [\text{L.mol}^{-1} \text{.cm}^{-1}])$			
$\lambda_{\text{fluo}} [\text{nm}]^b$	450	418	436
RQ_f^b	< 0.01	< 0.01	< 0.01
$\lambda_{\text{phos}} [\text{nm}]^c$	449	430	450
$E_T [\text{eV}]^{c,d}$	2.76	2.88	2.76
$\tau_p [\text{s}] (\lambda_{\text{em}} [\text{nm}])^c$	3.4 (449)	4.48 (73 %); 0.93 (27 %) (430)	3.1 (450)
$E_{\text{ox}} [\text{V}]^{e,f}$	0.96; 1.54; 1.69; 1.86	0.89; 1.61; 1.91	1.06; 1.23; 2.18
$E_{\text{red}} [\text{V}]^{e,g}$	-1.94; -2.63*; -3.01	-2.52; -2.62; -2.80	-1.98; -2.50; -2.79
HOMO [eV] ^h	-5.25	-5.16	-5.33
LUMO [eV] ^h	-2.60	-1.89	-2.55
$\Delta E_{\text{el}} [\text{eV}]^i$	2.65	3.27	2.78
$\mu_h [\text{cm}^2 \cdot \text{V}^{-1} \cdot \text{s}^{-1}]^j$	1.3×10^{-5}	1.0×10^{-4}	8.2×10^{-6}
$\mu_e [\text{cm}^2 \cdot \text{V}^{-1} \cdot \text{s}^{-1}]^j$	1.0×10^{-3}	3.2×10^{-3}	2.0×10^{-4}
$T_d [^\circ\text{C}]^k$	465	324	474
$T_g [^\circ\text{C}]^l$	169	136	143
$T_c [^\circ\text{C}]^l$	—	—	218
$T_f [^\circ\text{C}]^m$	254	232	303

*shoulder; a. in cyclohexane at RT; b. in cyclohexane at RT, $\lambda_{\text{exc}} = 310 \text{ nm}$; c. in 2-MeTHF at 77 K, $\lambda_{\text{exc}} = 310 \text{ nm}$; d. from $\lambda_{\text{phos max}}$; e. vs SCE; f. in CH₂Cl₂; g. in DMF; h. from electrochemical data; i. $\Delta E_{\text{el}} = |\text{HOMO-LUMO}|$; j. from SCLC; k. from TGA; l. from DSC (2nd heating cycle); m. from DSC (1st heating cycle) n.d.: not determined.

Thermal properties

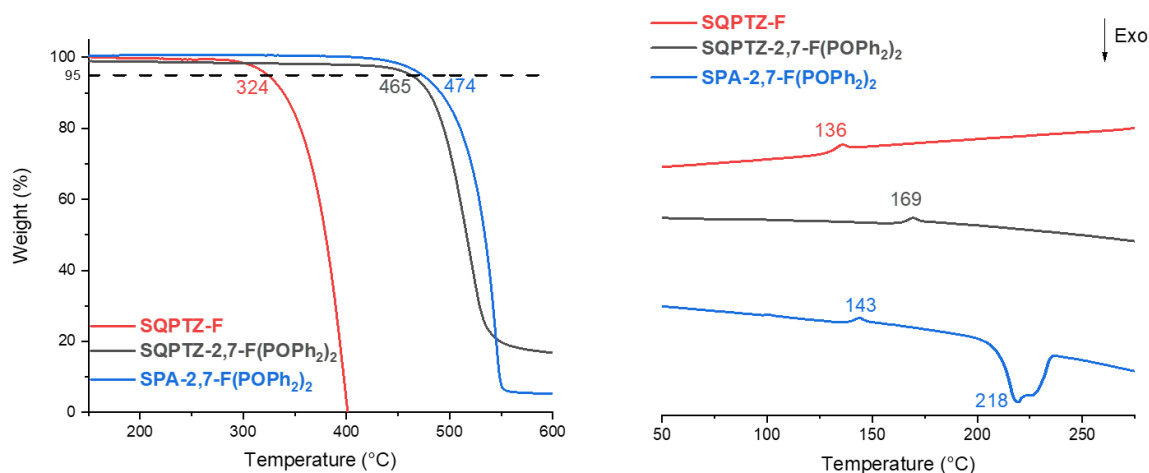


Figure 5. TGA and DSC traces of **SQPTZ-2,7-F(POPh₂)₂** (black lines), **SQPTZ-F** (red lines) and **SPA-2,7-F(POPh₂)₂** (blue lines)

The thermal properties have been studied by thermogravimetric analyses (TGA) and differential scanning calorimetry (DSC), Figure 5. The QPTZ/Diphenylphosphine oxide association found in **SQPTZ-2,7-F(POPh₂)₂** provides a very high decomposition temperature T_d (5% mass loss) (465°C), almost identical to that of **SPA-2,7-F(POPh₂)₂** (474°C). More importantly, **SQPTZ-2,7-F(POPh₂)₂** presents the highest glass transition temperature T_g (169°C, determined by DSC during the 2nd heating run, between 20 and 350°C). Both parameters are important to reach highly stable devices. Thus, incorporation of a sulphur atom in **SQPTZ-2,7-F(POPh₂)₂** rigidifies the structure compared to **SPA-2,7-F(POPh₂)₂**, improving in turn the thermal properties. It is important to mention that the model compound **SPA-2,7-F(POPh₂)₂** presents a crystallization temperature T_c at ca 218°C, which is suppressed in the two QPTZ based compounds **SQPTZ-2,7-F(POPh₂)₂** and **SQPTZ-F**. As amorphous materials are highly desired in this field, this is an important characteristic of the QPTZ fragment.

Charge transport properties

One of the key feature in the new generations of simplified SL-PhOLEDs is the capability of the host matrix to efficiently transport both type of charges, hole and electron.²³ As PhOLEDs are vertical stacks, space charge limited current (SCLC) devices are the most appropriate to probe the charge carrier mobilities. Herein, hole-only and electron-only devices have been fabricated and characterized providing the out-of-plane hole and electron mobilities respectively (Figure 6, see SI for technical details). The hole/electron mobility (μ_h/μ_e) of **SQPTZ-2,7-F(POPh₂)₂** have been estimated to be $1.3 \times 10^{-5} / 1.0 \times 10^{-3} \text{ cm}^2 \cdot \text{V}^{-1} \cdot \text{s}^{-1}$. For **SPA-2,7-F(POPh₂)₂**, the hole and electron mobilities have been previously reported at $8.2 \times 10^{-6} / 2.0 \times 10^{-4} \text{ cm}^2 \cdot \text{V}^{-1} \cdot \text{s}^{-1}$ in identical experimental conditions (Figure 5).⁴¹ One can note that the electron mobility of **SQPTZ-2,7-F(POPh₂)₂** is particularly high and five times higher than that of **SPA-2,7-F(POPh₂)₂**. On one hand, this can be considered as a positive feature as electron transport is often the weakest link in this technology. But, on the other hand, this is detrimental to the mobility balance between electrons and holes (μ_e/μ_h), ca 76 for **SQPTZ-2,7-F(POPh₂)₂**, vs 24 for **SPA-2,7-F(POPh₂)₂**, which is nowadays considered as a central prerequisite for a high performance SL-PhOLED (see a recent review on SL-PhOLEDs²³) Rationalizing this property is indeed important for the future of this technology. This is detailed below in the OLED section.

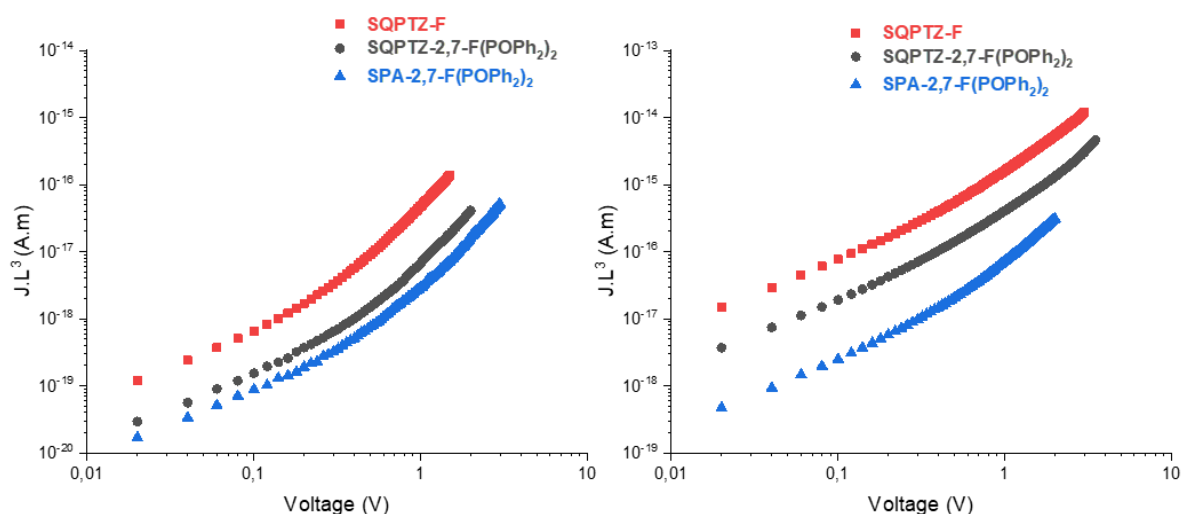


Figure 6. Thickness-scaled current voltage characteristics of **SQPTZ-2,7-F(POPh₂)₂** (black lines), **SQPTZ-F** (red lines) and **SPA-2,7-F(POPh₂)₂** (blue lines) hole-(Left) and

electron-only (Right) SCLC devices.

OLEDs characteristics

SQPTZ-2,7-F(POPh₂)₂ was finally incorporated as host in red, green and blue SL-PhOLEDs using as emitter either Ir(MDQ)₂(acac) for red emission, Ir(ppy)₃ and Ir(ppy)₂acac for green emission, and FIrpic for blue emission (Table 2, Figures 7). The SL-PhOLED architecture is the following: ITO/PEDOT:PSS (40 nm)/EML=Host+Guest 10% wt (100 nm)/LiF (1.2 nm)/Al (100 nm) with ITO/PEDOT:PSS as transparent anode and LiF/Al as metallic cathode. These data have been compared to the best host material reported to date, *i.e.* **SPA-2,7-F(POPh₂)₂** in order to explore the potential of the QPTZ fragment. As the device architecture is identical for both molecules, the different performance finds its origin only in the efficiency of the host material.

Considering the high E_T and suitable energy levels, **SQPTZ-2,7-F(POPh₂)₂** was first considered as host for blue PhOLEDs, which are still the most challenging today in terms of performances.^{9, 22-24, 52-54} In SL-PhOLEDs, only a few examples of blue emitting devices have been reported and almost all of them use the sky blue emitter FIrpic^{43, 55-58} (only one example is reported with a phosphor emitting at lower wavelength, *i.e.* FIr6⁴¹). **SQPTZ-2,7-F(POPh₂)₂** as host in a FIrpic-based device displays a moderate EQE of 8.4 % (at 22.9 mA/cm²) with nevertheless a low threshold voltage (V_{on}) of 2.4 V. The EQE and corresponding current (CE) and power (PE) efficiencies are lower than those reported for **SPA-2,7-F(POPh₂)₂**, in strictly identical conditions (Table 2). This can be assigned to the more balance mobilities of hole and electron measured for **SPA-2,7-F(POPh₂)₂** vs **SQPTZ-2,7-F(POPh₂)₂** (24 vs 76, see above). Indeed, when the charge transport is not well balanced, the recombination rate drops down and the EQE decreases. This can also lead to a shift of the recombination zone from the EML centre and to a resulting exciton quenching by the electrodes. This confirms that the ambipolarity of the host is undoubtedly one of the key parameters to control in order to reach high EQE SL-PhOLEDs. At 10 mA/cm², the difference between the two hosts is significantly less marked (EQE of 7.8 vs 12.5% for **SQPTZ-2,7-F(POPh₂)₂** and **SPA-2,7-F(POPh₂)₂** respectively). Two characteristics appear to be particularly interesting for **SQPTZ-2,7-F(POPh₂)₂** compare to **SPA-2,7-F(POPh₂)₂**: the threshold voltage and the maximum luminance ($V_{on} = 2.4$ vs 2.5 V and $L = 9901$ vs 8030 cd/m²). The V_{on} difference is due to the gap contraction observed in **SQPTZ-2,7-F(POPh₂)₂** and the higher luminance to the increased morphological stability (see above). These two characteristics are the direct consequences of the QPTZ fragment and will be exacerbated for the three other phosphors as detailed below.

The green SL-PhOLEDs have been then investigated in a similar way using two green emitters: the well-known Ir(ppy)₃ (HOMO: -4.97 eV/LUMO: -2.19 eV)⁴¹ and Ir(ppy)₂acac (HOMO: -5.06 eV/LUMO: -2.20 eV, see SI). Oppositely to the blue phosphor presented above, the performance difference between the two hosts is strongly less marked for Ir(ppy)₃ based devices (maximum EQE of 12.4 vs 16.4%, CE 43.4 vs 56.3 cd/A, 43.1 vs 53.6 lm/W for **SQPTZ-2,7-F(POPh₂)₂** and **SPA-2,7-F(POPh₂)₂**). The difference even decreases upon increasing the current density (at 10 mA/cm², an EQE of 9.7 % is measured for **SQPTZ-2,7-F(POPh₂)₂** vs 11.0 % for **SPA-2,7-F(POPh₂)₂**) in accordance with the higher stability of **SQPTZ-2,7-F(POPh₂)₂**. The same conclusions than those exposed above for FIrpic emitter, namely higher maximum luminance (ca 40000 cd/m²) and lower V_{on} (2.2 V) can also be drawn in this case, confirming the positive influence of the QPTZ fragment on these parameters.

The second green emitter Ir(ppy)₂acac leads to similar performance than those obtained with **SQPTZ-2,7-F(POPh₂)₂** / Ir(ppy)₃ with nevertheless a higher EQE at 10 mA/cm² (10.4 %) and a higher maximum luminance (ca 45000 cd/m²). The V_{on} appears in this case very low, recorded at 2.1 V, Table 2, translating a very efficient charge injection within the device.

For the red phosphor, the performance of both **SPA-2,7-F(POPh₂)₂** and **SQPTZ-2,7-F(POPh₂)₂** are, this time, almost identical with a maximum EQE around 8.5 %. The difference in term of maximum luminance is more pronounced with an increase of ca 30 % (6843 vs 9640 cd/m²) in favour of **SQPTZ-2,7-F(POPh₂)₂**. This high luminance recorded at a high current density of 240 mA/cm² (vs 170 mA/cm² for **SPA-2,7-F(POPh₂)₂**) translates the excellent stability of **SQPTZ-2,7-F(POPh₂)₂**. The V_{on} is also drastically reduced to 2.3 V (vs 2.8 V).

It should be finally stressed that all the devices exhibited red, green or blue emission arising exclusively from their corresponding iridium complex, showing an efficient energy transfer cascade (see electroluminescent spectra for all the device in Figure 7).

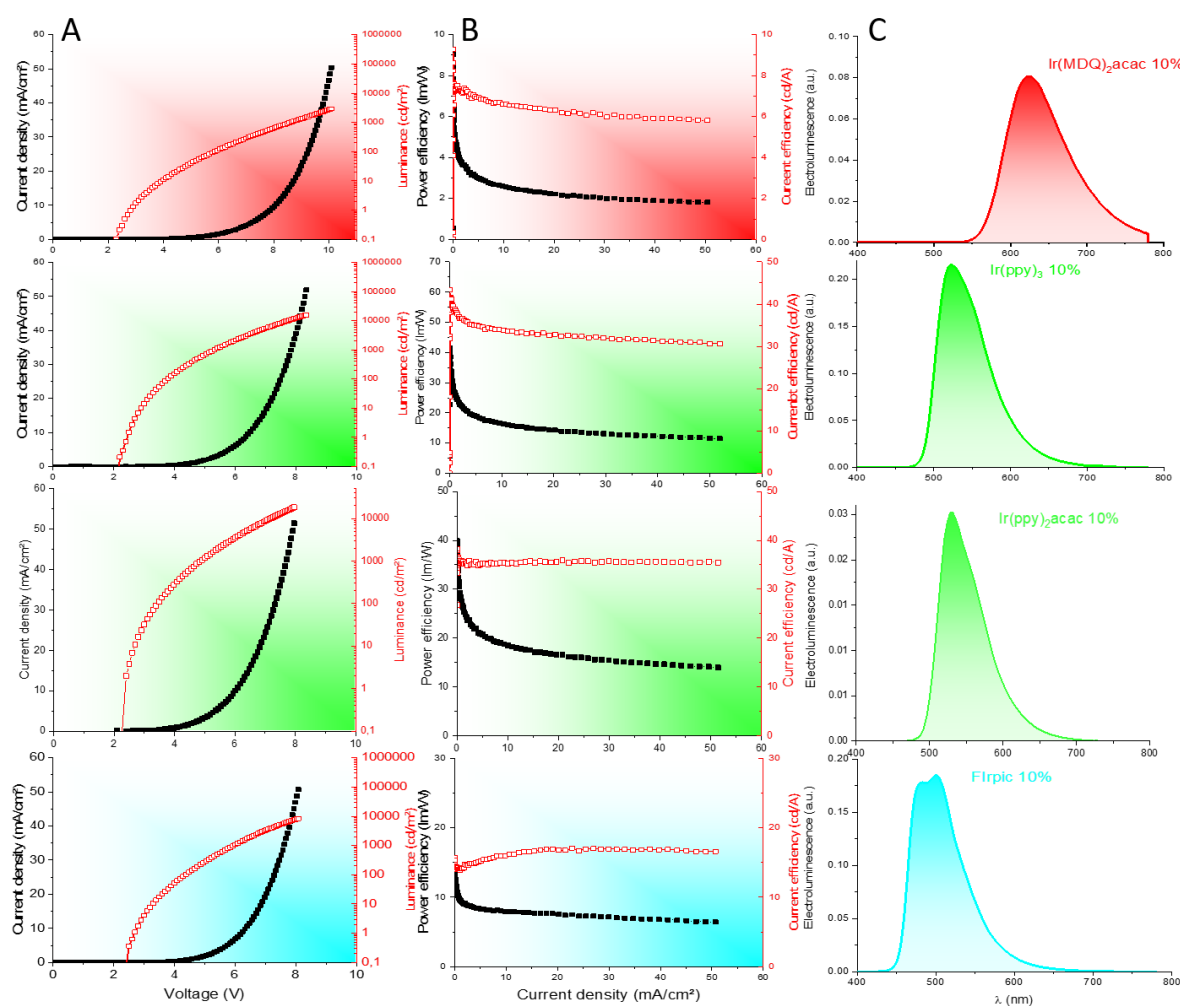


Figure 7. SL-PhOLEDs characteristics using **SQPTZ-2,7-F(POPh₂)₂** as host material. A) Current density (mA/cm²) and luminance (cd/m²) as a function of the voltage; B) Current efficiency (cd/A, filled symbols) and power efficiency (lm/W, empty symbol) as a function of the current density (mA/cm²) and C) Normalized EL spectra.

Table 2. Best SL-PhOLEDs performance using **SQPTZ-2,7-F(POPh₂)₂** as host material. **SPA-2,7-F(POPh₂)₂**⁴¹ is also reported for comparison purpose. Device structure: ITO/PEDOT:PSS (40 nm)/host + dopant (100 nm)/LiF (1.2 nm)/Al (100 nm). % of the phosphor used: 10% in mass. (E_T of Ir(MDQ)₂(acac) Ir(ppy)₃, Ir(ppy)₂acac and FIrpic are 2.08, 2.51, 2.46 and 2.72 eV in 2-Me-THF at 77 K).⁴¹

	V _{on} (V)	EQE (%)	CE (cd/A)	PE (lm/W)	EQE (%)	CE (cd/A)	PE (lm/W)	L _{max} (cd/m ²)	CIE coordinates (x ; y)
		At 10 mA/cm ²			Max (at J (mA/cm ²))			(at J (mA/cm ²))	
Red PhOLEDs (10% Ir(MDQ)₂(acac))									
SQPTZ-2,7-F(POPh₂)₂	2.3	5.6	6.6	2.6	8.4 (0.04)	9.3 (0.04)	8.6 (0.04)	9640 (240)	0.64 ; 0.36
SPA-2,7-F(POPh₂)₂	2.8	6.0	6.2	2.0	8.7 (0.03)	9.1 (0.03)	7.0 (0.03)	6843 (170)	0.64 ; 0.36
Green PhOLEDs (10% Ir(ppy)₃)									
SQPTZ-2,7-F(POPh₂)₂	2.2	9.7	33.8	16.3	12.4 (0.08)	43.4 (0.08)	41.3 (0.08)	40360 (220)	0.32 ; 0.63
SPA-2,7-F(POPh₂)₂	2.3	11.0	37.8	18.2	16.4 (0.04)	56.3 (0.04)	53.6 (0.04)	38970 (180)	0.31 ; 0.63
Green PhOLEDs (10% Ir(ppy)₂acac)									
SQPTZ-2,7-F(POPh₂)₂	2.1	10.4	35.3	18.4	11.3 (0.11)	38.3 (0.11)	38.8 (0.11)	44770 (220)	0.34 ; 0.63
SPA-2,7-F(POPh₂)₂									
Sky Blue PhOLEDs (10% FIrpic)									
SQPTZ-2,7-F(POPh₂)₂	2.4	7.8	16.0	7.9	8.4 (22.9)	17.1 (22.9)	7.5 (22.9)	9901 (100)	0.18 ; 0.43
SPA-2,7-F(POPh₂)₂	2.5	12.5	27.3	14.5	18.0 (0.04)	39.0 (0.04)	38.4 (0.04)	8030 (80)	0.15 ; 0.37

To sum up, compared to the best universal host reported to date, namely **SPA-2,7-F(POPh₂)₂**, the new host material **SQPTZ-2,7-F(POPh₂)₂** incorporating the QPTZ fragment presents similar EQE for the red devices and lower EQE for the green and blue devices. The less balanced charge transport between electron and hole is surely at the origin of the different EQE. However, the particularity of the QPTZ unit has been clearly highlighted and this fragment displays very interesting properties for SL-PhOLEDs. In all the cases, the V_{on} of **SQPTZ-2,7-F(POPh₂)₂** based devices are reported lower than those of **SPA-2,7-F(POPh₂)₂** ones. The highest difference, 0.5 V, is observed for the red devices. This is an important characteristic in this technology, which translates the electrochemical gap difference between the two molecules (2.78 vs 2.65 eV). In addition, for all the phosphors investigated, the

maximum luminances of **SQPTZ-2,7-F(POPh₂)₂** based devices are higher than those of **SPA-2,7-F(POPh₂)₂** based devices, demonstrating a good stability at high current density. A very high luminance of 45000 cd/m² is particularly detected for the Ir(ppy)₂acac phosphor. Thus, thanks to high HOMO energy level and good stability at a high current density, the QPTZ fragment is at the origin of the low V_{on} and the high luminances obtained.

Conclusion

In this work, we have investigated the potential of the quinolinophenothiazine (QPTZ) fragment used in a host material for simplified SL-PhOLEDs. The QPTZ core has been attached to an efficient acceptor unit, namely diphenylphosphineoxide-fluorene through a classical *D-spiro-A* design. **SQPTZ-2,7-F(POPh₂)₂** has been successfully incorporated in red, green and blue SL-PhOLEDs with an average EQE of ca 10%. The luminances reached were high and above those reported with the best host material used in date in SL-PhOLEDs, namely **SPA-2,7-F(POPh₂)₂**. This means that **SQPTZ-2,7-F(POPh₂)₂** based devices can support a higher current density than those based on **SPA-2,7-F(POPh₂)₂**. Thanks to its high HOMO energy level, the QPTZ unit also allows to decrease the threshold voltage of the corresponding devices, which is a key point in '*single-layer*' technology. Thanks to these two appealing characteristics, QPTZ appears as a promising building unit and can advance the field of organic semi-conducting materials. We are convinced that the future development of QPTZ-based materials would also be appealing for other organic devices.

Supporting Information

Details on the materials synthesis, their structural, thermal and electrochemical properties, theoretical modeling and device data are provided in the supporting Information. Copies of NMR spectra are also included. The Supporting Information is available free of charge on the Publications website.

Acknowledgments

The authors would like to thank the ANR (SPIROQUEST, n°19-CE05-0024) for financial support of this project, the Région Bretagne (DIADEM project) for PhD grant (FL) and the Agence de l'environnement et de la maîtrise de l'énergie (ADEME) for PhD grand (CB, EcoElec Project). We would like to thank the CRMPO (Rennes) for mass analysis. This work was granted access to the HPC resources of CINES under the allocation 2021-A0100805032 awarded by GENCI. The authors thank Dr J. F. Bergamini (Rennes) for the TOC material.

Received: ((will be filled in by the editorial staff))
Published online: ((will be filled in by the editorial staff)).

References

1. Gsänger, M.; Bialas, D.; Huang, L.; Stolte, M.; Würthner, F., Organic Semiconductors based on Dyes and Color Pigments. *Adv. Mater.* 2016, **28**, 3615.

2. Suraru, S.-L.; Würthner, F., Strategies for the Synthesis of Functional Naphthalene Diimides. *Angew. Chem. Int. Ed.* 2014, **53**, 7428.
3. Wang, C.; Dong, H.; Hu, W.; Liu, Y.; Zhu, D., Semiconducting π -Conjugated Systems in Field-Effect Transistors: A Material Odyssey of Organic Electronics *Chem. Rev.* 2012, **112**, 2208.
4. Yook, K. S.; Lee, J. Y., Organic Materials for Deep Blue Phosphorescent Organic Light-Emitting Diodes. *Adv. Mater.* 2012, **24**, 3169.
5. Romain, M.; Tondelier, D.; Jeannin, O.; Geffroy, B.; Rault-Berthelot, J.; Poriel, C., Properties modulation of organic semi-conductors based on a donor-spiro-acceptor (D-spiro-A) molecular design: new host materials for efficient sky-blue PhOLEDs. *J. Mater. Chem. C* 2015, **3**, 97010.
6. Méhes, G.; Nomura, H.; Zhang, W.; Nakagawa, T.; Adachi, C., Enhanced Electroluminescence Efficiency in a Spiro-Acridine Derivative through Thermally Activated Delayed Fluorescence *Angew. Chem. Int. Ed.* 2012, **51**, 11311.
7. Lucas, F.; Ibraikulov, O. A.; Quinton, C.; Sicard, L.; Heiser, T.; Tondelier, D.; Geffroy, B.; Leclerc, N.; Rault-Berthelot, J.; Poriel, C., Spirophenylacridine-2,7-(diphenylphosphineoxide)-fluorene: A Bipolar Host for High-Efficiency Single-Layer Blue Phosphorescent Organic Light-Emitting Diodes. *Adv. Opt. Mater.* 2020, **8**, 1901225.
8. Zou, S.-N.; Chen, X.; Yang, S.-Y.; Kumar, S.; Qu, Y.-K.; Yu, Y.-J.; Fung, M.-K.; Jiang, Z.-Q.; Liao, L.-S., Efficient Violet Organic Light-Emitting Diodes with CIEy of 0.02 Based on Spiro Skeleton. *Adv. Opt. Mater.* 2020, **8**, 2001074.
9. Peng, C. C.; Yang, S. Y.; Li, H. C.; Xie, G. H.; Cui, L. S.; Zou, S. N.; Poriel, C.; Jiang, Z. Q.; Liao, L. S., Highly Efficient Thermally Activated Delayed Fluorescence via an Unconjugated Donor-Acceptor System Realizing EQE of Over 30%. *Adv. Mater.* 2020, **32**, 2003885.
10. Khan, A.; Chen, X.; Kumar, S.; Yang, S.-Y.; Yu, Y.-J.; Luo, W.; Jiang, Z.-Q.; Fung, M.-K.; Liao, L.-S., Spiro-type host materials with rigidified skeletons for RGB phosphorescent OLEDs. *J. Mater. Chem. C* 2020, **8**, 12470.
11. Tang, X.; Liu, X.-Y.; Yuan, Y.; Wang, Y.-J.; Li, H.-C.; Jiang, Z.-Q.; Liao, L.-S., High-Efficiency White Organic Light-Emitting Diodes Integrating Gradient Exciplex Allocation System and Novel D-Spiro-A Materials. *ACS Appl. Mater. Interfaces* 2018, **10**, 29840.
12. Thiery, S.; Tondelier, D.; Geffroy, B.; Jeannin, O.; Rault-Berthelot, J.; Poriel, C., Modulation of the Physicochemical Properties of Donor–Spiro–Acceptor Derivatives through Donor Unit Planarisation: Phenylacridine versus Indoloacridine—New Hosts for Green and Blue Phosphorescent Organic Light-Emitting Diodes (PhOLEDs). *Chem. Eur. J.* 2016, **22**, 10136.
13. Zhang, Y.-X.; Ding, L.; Liu, X.-Y.; Chen, H.; Ji, S.-J.; Liao, L.-S., Spiro-fused N-phenylcarbazole-based host materials for blue phosphorescent organic light-emitting diodes. *Org. Electron.* 2015, **20**, 112.
14. Zhang, D.; Shen, W.; Sun, H.; He, R.; Li, M., Theoretical Investigations of the Spiro-Annulated Triphenylamine/ N-Phenylcarbazole-Based Ambipolar Host Materials for OLEDs. *ChemistrySelect* 2017, **2**, 6604.
15. Seo, J.-A.; Gong, M. S.; Lee, J. Y., Thermally stable indoloacridine type host material for high efficiency blue phosphorescent organic light-emitting diodes. *Org. Electron.* 2014, **15**, 3773.

16. Poriel, C.; Rault-Berthelot, J.; Thiery, S.; Quinton, C.; Jeannin, O.; Biapo, U.; Geffroy, B.; Tondelier, D., 9H-Quinolino[3,2,1-k]phenothiazine: A New Electron-Rich Fragment for Organic Electronics. *Chem. Eur. J.* 2016, **22**, 17930.
17. Quinton, C.; Sicard, L.; Jeannin, O.; Vanthuyne, N.; Poriel, C., Confining Nitrogen Inversion to Yield Enantiopure Quinolino[3,2,1-k]Phenothiazine Derivatives. *Adv. Funct. Mat.* 2018, **28**, 180340.
18. Wang, Y.-K.; Li, S.-H.; Wu, S.-F.; Huang, C.-C.; Kumar, S.; Jiang, Z.-Q.; Fung, M.-K.; Liao, L.-S., Tilted Spiro-Type Thermally Activated Delayed Fluorescence Host for $\approx 100\%$ Exciton Harvesting in Red Phosphorescent Electronics with Ultralow Doping Ratio. *Adv. Funct. Mater.* 2018, **28**, 1706228.
19. Wang, Y.-K.; Wu, S.-F.; Yuan, Y.; Li, S.-H.; Fung, M.-K.; Liao, L.-S.; Jiang, Z.-Q., Donor- σ -Acceptor Molecules for Green Thermally Activated Delayed Fluorescence by Spatially Approaching Spiro Conformation. *Org. Lett.* 2017, **19**, 3155.
20. Wang, Y.-K.; Huang, C.-C.; Ye, H.; Zhong, C.; Khan, A.; Yang, S.-Y.; Fung, M.-K.; Jiang, Z.-Q.; Adachi, C.; Liao, L.-S., Through Space Charge Transfer for Efficient Sky-Blue Thermally Activated Delayed Fluorescence (TADF) Emitter with Unconjugated Connection. *Adv. Opt. Mater.* 2020, **8**, 1901150.
21. Hellwinkel, D.; Schmid, W., Modifizierte Tetrahelicen-Systeme, III. Zweifach ortho-verbrückte Triphenylamin-Derivate. *Chem. Ber.* 1980, **113**, 358.
22. Poriel, C.; Rault - Berthelot, J., Blue Single-Layer Organic Light-Emitting Diodes Using Fluorescent Materials: A Molecular Design View Point. *Adv. Funct. Mat.* 2020, **30**, 1910040.
23. Poriel, C.; Rault - Berthelot, J., Designing Host Materials for the Emissive Layer of Single-Layer Phosphorescent Organic Light-Emitting Diodes: Toward Simplified Organic Devices. *Adv. Funct. Mat.* 2021, **31**, 2010547.
24. Wang, Q.; Lucas, F.; Quinton, C.; Qu, Y.-K.; Rault-Berthelot, J.; Jeannin, O.; Yang, S.-Y.; Kong, F.-C.; Kumar, S.; Liao, L.-S.; Poriel, C.; Jiang, Z.-Q., Evolution of pure hydrocarbon hosts: simpler structure, higher performance and universal application in RGB phosphorescent organic light-emitting diodes. *Chem. Sci.* 2020, **11**, 4887.
25. Maheshwaran, A.; Sree, V. G.; Park, H.-Y.; Kim, H.; Han, S. H.; Lee, J. Y.; Jin, S.-H., High Efficiency Deep-Blue Phosphorescent Organic Light-Emitting Diodes with CIE x, y (≤ 0.15) and Low Efficiency Roll-Off by Employing a High Triplet Energy Bipolar Host Material. *Adv. Funct. Mater.* 2018, **28**, 1802945.
26. Li, W.; Li, J.; Liu, D.; Jin, Q., Simple Bipolar Host Materials for High-Efficiency Blue, Green, and White Phosphorescence OLEDs. *ACS Appl. Mater. Interfaces.* 2016, **8**, 22382.
27. Huang, J.-J.; Hung, Y.-H.; Ting, P.-L.; Tsai, Y.-N.; Gao, H.-J.; Chiu, T.-L.; Lee, J.-H.; Chen, C.-L.; Chou, P.-T.; Leung, M.-k., Orthogonally Substituted Benzimidazole-Carbazole Benzene As Universal Hosts for Phosphorescent Organic Light-Emitting Diodes. *Org. Lett.* 2016, **18**, 672.
28. Ding, L.; Dong, S.-C.; Jiang, Z.-Q.; Chen, H.; Liao, L. S., Orthogonal Molecular Structure for Better Host Material in Blue Phosphorescence and Larger OLED White Lighting Panel. *Adv. Funct. Mater.* 2015, **25**, 645.
29. Cui, L.-S.; Xie, Y.-M.; Wang, Y.-K.; Zhong, C.; Deng, Y.-L.; Liu, X.-Y.; Jiang, Z.-Q.; Liao, L.-S., Pure Hydrocarbon Hosts for $\approx 100\%$ Exciton Harvesting in Both Phosphorescent and Fluorescent Light-Emitting Devices. *Adv. Mater.* 2015, **27**, 4213.

30. Udagawa, K.; Sasabe, H.; Cai, C.; Kido, J., Low-Driving-Voltage Blue Phosphorescent Organic Light-Emitting Devices with External Quantum Efficiency of 30%. *Adv. Mater.* 2014, **26**, 5062.
31. Im, Y.; Byun, S. Y.; Kim, J. H.; Lee, D. R.; Oh, C. S.; Yook, K. S.; Lee, J. Y., Recent Progress in High-Efficiency Blue-Light-Emitting Materials for Organic Light-Emitting Diodes. *Adv. Funct. Mater.* 2017, **27**, 1603007.
32. Lee, C. W.; Lee, J. Y., Above 30% External Quantum Efficiency in Blue Phosphorescent Organic Light-Emitting Diodes Using Pyrido[2,3-*b*]indole Derivatives as Host Materials. *Adv. Mater.* 2013, **25**, 5450.
33. Kim, M.; Lee, J. Y., Engineering of Interconnect Position of Bicarbazole for High External Quantum Efficiency in Green and Blue Phosphorescent Organic Light-Emitting Diodes. *ACS Appl. Mater. Interfaces* 2014, **6**, 14874.
34. Liu, X.-Y.; Tang, X.; Zhao, Y.; Zhao, D.; Fan, J.; Liao, L.-S., Dispiro and Propellane: Novel Molecular Platforms for Highly Efficient Organic Light-Emitting Diodes. *ACS Appl. Mater. Interfaces* 2018, **10**, 1925.
35. Kim, K.-H.; Lee, S.; Moon, C.-K.; Kim, S.-Y.; Park, Y.-S.; Lee, J.-H.; Woo Lee, J.; Huh, J.; You, Y.; Kim, J.-J., Phosphorescent dye-based supramolecules for high-efficiency organic light-emitting diodes. *Nat. Comm.* 2014, **5**, 4769.
36. Chen, W.-C.; Yuan, Y.; Zhu, Z.-L.; Jiang, Z.-Q.; Su, S.-J.; Liao, L.-S.; Lee, C.-S., De novo design of D- σ -A molecules as universal hosts for monochrome and white phosphorescent organic light-emitting diodes. *Chem. Sci.* 2018, **9**, 4062.
37. Song, W.; Shi, L.; Gao, L.; Hu, P.; Mu, H.; Xia, Z.; Huang, J.; Su, J., [1,2,4]Triazolo[1,5-*a*]pyridine as Building Blocks for Universal Host Materials for High-Performance Red, Green, Blue and White Phosphorescent Organic Light-Emitting Devices. *ACS Appl. Mater. Interfaces* 2018, **10**, 5714.
38. Chang, S.-y.; Lin, G.-T.; Cheng, Y.-C.; Huang, J.-J.; Chang, C.-L.; Lin, C.-F.; Lee, J.-H.; Chiu, T.-L.; Leung, M.-k., Construction of Highly Efficient Carbazol-9-yl-Substituted Benzimidazole Bipolar Hosts for Blue Phosphorescent Light-Emitting Diodes: Isomer and Device Performance Relationships. *ACS Appl. Mater. Interfaces* 2018, **10**, 42723.
39. Park, H.-Y.; Maheshwaran, A.; Moon, C.-K.; Lee, H.; Reddy, S. S.; Sree, V. G.; Yoon, J.; Kim, J. W.; Kwon, J. H.; Kim, J.-J.; Jin, S.-H., External Quantum Efficiency Exceeding 24% with CIE_y Value of 0.08 using a Novel Carbene-Based Iridium Complex in Deep-Blue Phosphorescent Organic Light-Emitting Diodes. *Adv. Mater.* 2020, **32**, 2002120.
40. Cheng, T.-Y.; Lee, J.-H.; Chen, C.-H.; Chen, P.-H.; Wang, P.-S.; Lin, C.-E.; Lin, B.-Y.; Lan, Y.-H.; Hsieh, Y.-H.; Huang, J.-J.; Lu, H.-F.; Chao, I.; Leung, M.-k.; Chiu, T.-L.; Lin, C.-F., Carrier Transport and Recombination Mechanism in Blue Phosphorescent Organic Light-Emitting Diode with Hosts Consisting of Cabazole- and Triazole-Moiety. *Scientific Reports* 2019, **9**, 3654.
41. Lucas, F.; Quinton, C.; Fall, S.; Heiser, T.; Tondelier, D.; Geffroy, B.; Leclerc, N.; Rault-Berthelot, J.; Poriel, C., Universal host materials for red, green and blue high-efficiency single-layer phosphorescent organic light-emitting diodes. *J. Mater. Chem. C* 2020, **8**, 16354.
42. Yoshii, A.; Onaka, Y.; Ikemoto, K.; Izumi, T.; Sato, S.; Kita, H.; Taka, H.; Isobe, H., Acyclic, linear oligo-meta-phenylenes as multipotent base materials for highly efficient single-layer organic light-emitting devices. *Chem. Asian J.* 2020, **15**, 2181.

43. Hsu, F.-M.; Chien, L.-J.; Chen, K.-T.; Li, Y.-Z.; Liu, S.-W., High morphology stability and ambipolar transporting host for use in blue phosphorescent single-layer organic light-emitting diodes. *Org. Electron.* 2014, **15**, 3327.
44. Jang, S. E.; Joo, C. W.; Lee, J. Y., High quantum efficiency in simple blue phosphorescent organic light-emitting diodes without any electron injection layer. *Thin Solid Films* 2010, 906.
45. Poriel, C.; Ferrand, Y.; Le Maux, P.; Rault-Berthelot, J.; Simonneaux, G., Organic Cross-Linked Electropolymers as Supported Oxidation Catalysts: Poly((tetrakis(9,9'-spirobifluorenyl)porphyrin)manganese) Films. *Inorg. Chem.* 2004, **43**, 5086.
46. Poriel, C.; Ferrand, Y.; Le Maux, P.; Paul-Roth, C.; Simonneaux, G.; Rault-Berthelot, J., Anodic oxidation and physicochemical properties of various porphyrin-fluorenes or -spirobifluorenes: Synthesis of new polymers for heterogeneous catalytic reactions. *J. Electroanal. Chem.* 2005, **583**, 92.
47. Rault-Berthelot, J.; Poriel, C.; Justaud, F.; Barrière, F., Anodic oxidation of indenofluorene. Electrodeposition of electroactive poly(indenofluorene). *New J. Chem.* 2008, **32**, 1259.
48. Poriel, C.; Rault-Berthelot, J.; Thirion, D., Modulation of the Electronic Properties of 3π -2spiro Compounds Derived from Bridged Oligophenylenes: A Structure–Property Relationship. *J. Org. Chem.* 2013, **73**, 886.
49. Thiery, S.; Tondelier, D.; Geffroy, B.; Jacques, E.; Robin, M.; Métivier, R.; Jeannin, O.; Rault-Berthelot, J.; Poriel, C., Spirobifluorene-2,7-dicarbazole-4'-phosphine Oxide as Host for High-Performance Single-Layer Green Phosphorescent OLED Devices. *Org. Lett.* 2015, **17**, 4682.
50. Sicard, L.; Quinton, C.; Peltier, J.-D.; Tondelier, D.; Geffroy, B.; Biapo, U.; Métivier, R.; Jeannin, O.; Rault-Berthelot, J.; Poriel, C., Spirobifluorene Regioisomerism: A Structure–Property Relationship Study. *Chem. Eur. J.* 2017, **23**, 7719.
51. Sicard, L. J.; Li, H.-C.; Wang, Q.; Liu, X.-Y.; Jeannin, O.; Rault-Berthelot, J.; Liao, L.-S.; Jiang, Z.-Q.; Poriel, C., C1-Linked Spirobifluorene Dimers: Pure Hydrocarbon Hosts for High-Performance Blue Phosphorescent OLEDs. *Angew. Chem. Int. Ed.* 2019, **58**, 3848.
52. Mertens, R., *The OLED Handbook: A Guide to OLED Technology, Industry & Market*. 2019 edition.
53. Lee, J.-H.; Chen, C.-H.; Lee, P.-H.; Lin, H.-Y.; Leung, M.-k.; Chiu, T.-L.; Lin, C.-F., Blue organic light-emitting diodes: current status, challenges, and future outlook. *J. Mater. Chem. C* 2019, **7**, 5874.
54. Wang, Y.; Yun, J. H.; Wang, L.; Lee, J. Y., High Triplet Energy Hosts for Blue Organic Light- Emitting Diodes. *Adv. Funct. Mater.* 2020, 2008332.
55. Liu, Y.; Cui, L.-S.; Xu, M.-F.; Shi, X.-B.; Zhou, D.-Y.; Wang, Z.-K.; Jiang, Z.-Q.; Liao, L. S., Highly efficient single-layer organic light-emitting devices based on a bipolar pyrazine/carbazole hybrid host material. *J. Mater. Chem. C* 2014, **2**, 2488.
56. Chang, H.-H.; Tsai, W.-S.; Chang, C.-P.; Chen, N.-P.; Wong, K.-T.; Hung, W.-Y.; Chen, S.-W., A new tricarbazole phosphine oxide bipolar host for efficient single-layer blue PhOLED. *Org. Electron.* 2011, **12**, 2025.
57. Liu, Z.; Helander, M. G.; Wang, Z.; Lu, Z., Efficient single layer RGB phosphorescent organic light-emitting diodes. *Org. Electron.* 2009, **10**, 1146.

58. Yin, Y.; Wen, X.; Yu, J.; Zhang, L.; Xie, W., Single layer blue pholed. *IEEE Photonics Technology Letters* 2013, **25**, 1041.